Pergamon

Journal of Structural Geology, Vol. 17, No. 6, pp. 863 to 873, 1995
Elsevier Science Ltd
Printed in Great Britain

0191-8141(94)00105-7

Fractal nature and scaling of normal faults in the Española Basin, Rio Grande rift, New Mexico: implications for fault growth and brittle strain

K. E. CARTER

Los Alamos National Lab, EES-1 D462, Los Alamos, NM 87545, U.S.A.

and

C. L. WINTER

Los Alamos National Lab, CIC-3 B265, Los Alamos, NM 87545, U.S.A.

(*Received* 18 *May* 1994; *accepted in revised form* 27 *September* 1994)

Abstract—Quaternary faults in the western Española Basin of the Rio Grande rift show a power-law size (displacement) distribution suggesting that faulting in this region is scale invariant, and that faults are self similar. The power law, or fractal, distribution is characterized by a fractal dimension of 0.66 to 0.79 and represents a young, immature, active fault population in a continental extensional regime. Based on this distribution, it is estimated that unobserved faults with very small displacements account for up to 6% of the total strain. Since 1.2 Ma, total extension in this part of the basin has been at least 5%.

A direct correlation exists between maximum displacement and length of faults in this area suggesting that they obey a scaling relationship in which the ratio of $\log d_{max}/\log L$, is 5×10^{-3}. This ratio is nearly constant for faults whose lengths span three-orders of magnitude, indicating that there is no difference in the scaling relationship of displacement and length between faults of all sizes. Considering previous models, these fault characteristics suggest that, in the western Española Basin: (1) host rock shear strengths are low; (2) remote shear stresses were probably high; and (3) most faults do not extend throughout the brittle crust. Finally, displacement profiles on five of the largest faults are asymmetric and show a rapid decrease in displacement from the point of maximum displacement toward the fault tip.

The fractal nature, scaling relationship and distribution of displacement on faults are used to suggest that faults grew by nearly proportional increases in displacement and length, perhaps by mechanisms dominated by propagating shear fractures rather than by linkage of pre-existing joints or faults.

INTRODUCTION

Recently, considerable attention has been devoted to the characterization of fault populations for the purpose of understanding fault formation, growth and strain. Approaches to gaining such an understanding include, for example, determining scaling laws and the size-frequency distributions of fault arrays. Presently, the size-frequency distributions of many fault populations are being recognized as fractal in nature. The fractal concept was developed by Mandelbrot (1967, 1982) and is based on the centuries-old observation that many features, such as folds and faults, appear the same at different scales. Embedded in Mandelbrot's fractal concept is the means mathematically to describe the size-frequency relationship of objects, such as faults. Such a relationship obeys a power-law and implies scale-invariance and statistical self-similarity of the described objects. It is, in part, quantification of this relationship through fractal analysis (Turcotte 1989) that allows a more fundamental understanding of faults and the processes responsible for their formation and growth.

In recent years, there has been a virtual explosion of interest in this topic (e.g. Turcotte 1986, Watterson 1986, Walsh *et al.* 1991, Cowie & Scholz 1992a,b, Gillespie *et al.* 1992, Hatton *et al.* 1993). For example, fractal analysis of faults has been used to understand the relationship between brittle structure and seismicity (Hatton *et al.* 1993), fracture formation and depth (Barton & Zoback 1992), and faulting and strain (Scholz & Cowie 1990, Walsh *et al.* 1991, Marrett & Allmendinger 1992). Several researchers have documented different scaling relationships for faults in different tectonic and lithologic domains (e.g. see Cowie & Scholz 1992b), and, in some cases there is evidence that large and small faults might have different scaling laws ('fractal tear' of Scholz & Aviles 1986, Turcotte 1989, 'cross over' of Cowie & Scholz 1992a, 'multifractal' compressional duplexes of Wojtal 1994). These results have evoked different explanations for fault growth which include concepts such as self-similar and self-affine growth, as well as the dependence on variables such as host rock properties and remote shear stress (e.g. Watterson 1986, Cowie & Scholz 1992a). Results from distribution analysis have also produced opposing opinions on the significance or contribution of small, unobserved faults to the total strain (Scholz & Cowie 1990, Walsh *et al.* 1991, Marrett & Allmendinger 1992): if large and small faults have different scaling laws, extrapolation toward smaller dimensions (e.g. trace length and termination depth) and displacements will not be valid.

The existence of these many different models probably depends, in part, on the nature of the faults, sampling procedure and tectonic setting. Therefore, in

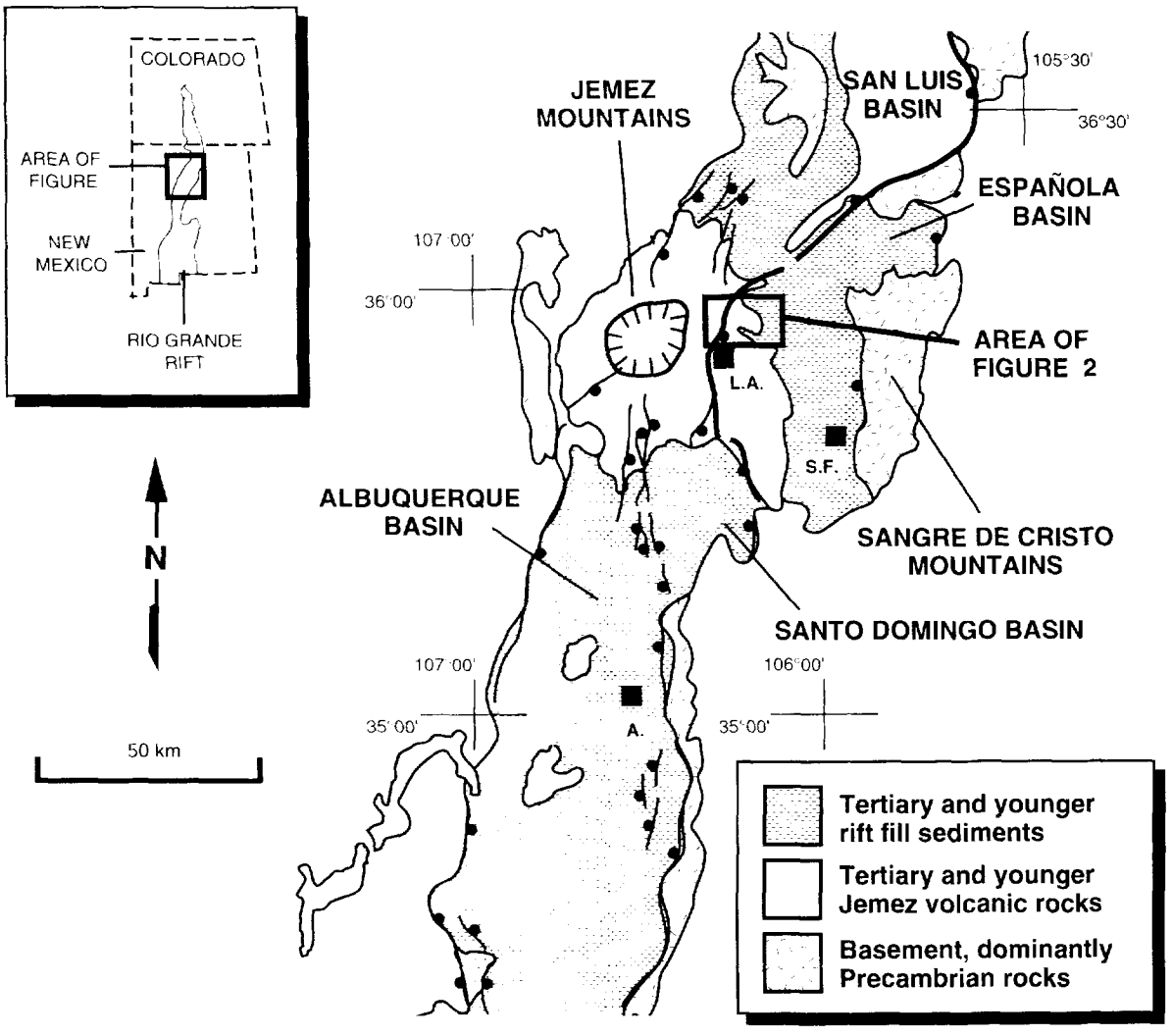

Fig. 1. Generalized tectonic map of the Rio Grande rift in North New Mexico (from Gardner & Goff 1984). LA—Los Alamos, SF—Santa Fe, A—Albuquerque. Heavy lines are faults: west of LA = Pajarito master fault zone, south of San Luis Basin = Embudo fault zone.

an effort to place constraints on some of these models to understand better the physical processes during fault growth, we present analyses of a suite of Quaternary normal faults from within an active continental rift, and characterize the nature of the relationships between fault dimensions and displacements. We address the statistical and geological significance of the fractal analysis used in that characterization and discuss the tectonic implications. Specifically, we present: (1) scaling laws for a previously unanalyzed population of young normal faults in a rift environment; (2) implications for fault growth models in this area, in particular, addressing self-similar growth implied by the population; and (3) estimates for the total strain in this part of the basin, considering the contribution of small or unobserved faults.

GEOLOGIC SETTING

The Española Basin is located in the Rio Grande rift in northern New Mexico, U.S.A. It lies south of the San Luis Basin and north of the Albuquerque basin (Fig. 1). The northern and western basin margins are defined by the Embudo and Pajarito fault zones (Gardner & Goff 1984), respectively. The topography of the western part of the basin consists of mesas and canyons formed in the Pleistocene Bandelier Tuff. The Bandelier Tuff comprises a series of ash fall deposits and ignimbrites that were deposited between 1.61 Ma and 1.22 Ma (Izett & Obradovich 1994) during the eruption of the Valles caldera. The Bandelier Tuff consists of two members: each is composed of a thick composite ash flow sheet over a basal ash fall bed (Bailey *et al.* 1969) and both members vary from very densely to poorly welded (Bailey *et al.* 1969, Gardner *et al.* 1986). Tertiary sedimentary and volcanic rocks underlie the Bandelier Tuff (Fig. 2) and in many places thin patchy Holocene sediments overlie the Tuff.

The western part of the basin is dissected by five major, roughly N-trending fault zones (Fig. 2) that displace rocks as young as Bandelier Tuff and overlying Holocene sediments. The western basin-bounding fault, the Pajarito fault zone, formed as early as 5 Ma (Manley 1979, Aldrich 1986) probably in response to roughly EW (Aldrich *et al.* 1986) to ENE-directed (Carter &

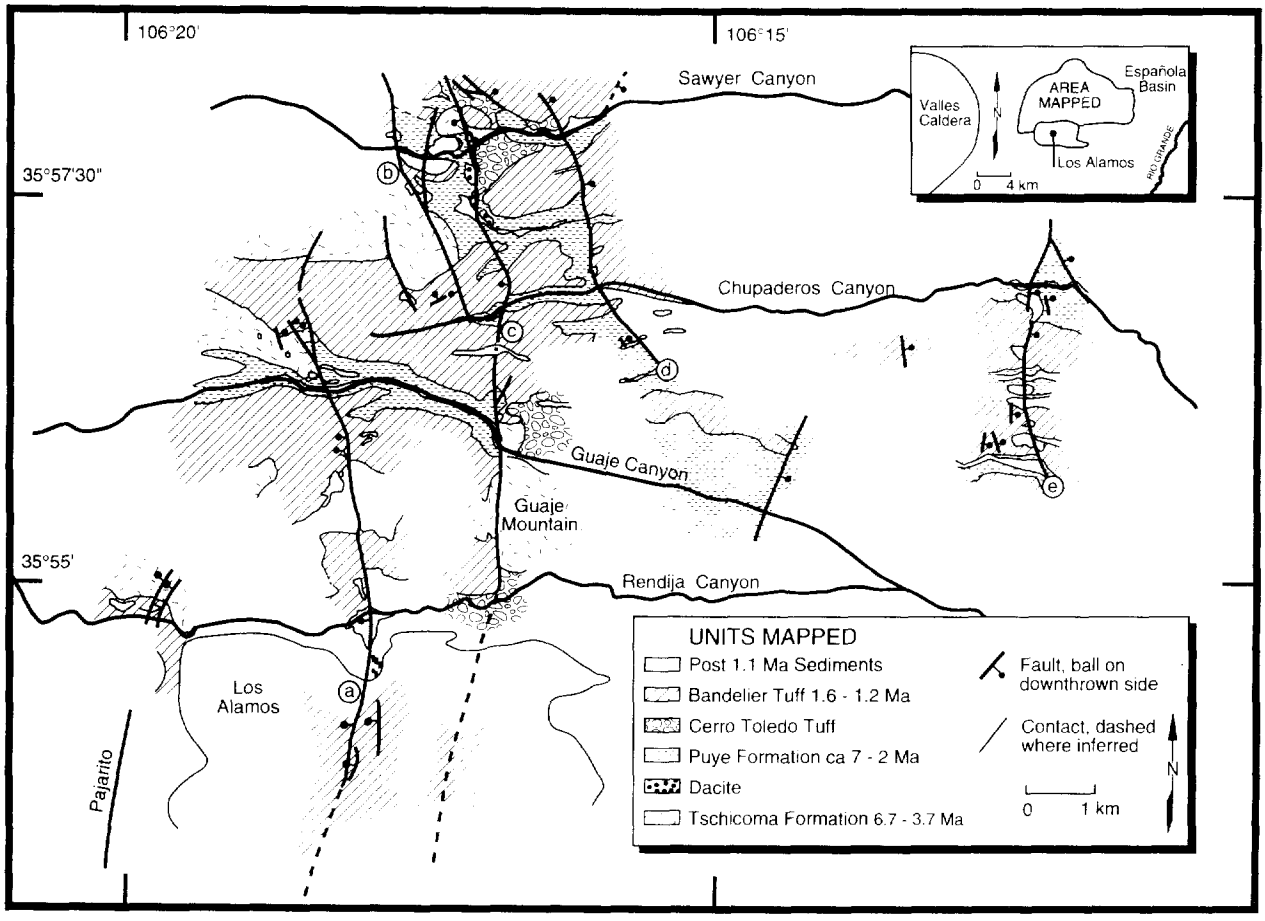

Fig. 2. Structural map of western Española Basin, New Mexico. Heavy lines are fault traces. Dashed lines are fracture (process) zones. a = Rendija Canyon fault, b = unnamed fault, c = Guaje Mountain fault, d = Sawyer Canyon fault, e = Puye fault. Faults with $d < 2$ m or unknown lengths are not shown.

Gardner 1993) extension. Vertical offset varies along the zone and has an estimated maximum displacement of 200 m, down to the east (Gardner & House 1987). Since 1.2 Ma, at least the northern segment of the Pajarito fault has experienced approximately 125–200 m of vertical displacement as determined from the E-facing scarp that offsets the youngest member of the Bandelier Tuff (Gardner & House 1987).

Four fault zones east of the master Pajarito fault trend roughly north and dip steeply east or west. Debris flows containing 10 ka (Wong *et al.* in preparation) to 4 ka (Gardner *et al.* 1990) charcoal are faulted, indicating that movement on two faults closest to the Pajarito has continued through the Holocene. The Bandelier Tuff is offset across all four faults indicating maximum vertical displacement ranging up to 40 m on individual faults.

The western part of the Española Basin in which these faults occur provides an excellent opportunity to analyze the relationships between several dimensions of the faults: the region provides unusual exposures in mesa/canyon topography and contains many fault zones of different sizes that cut young, cliff-forming host rocks. Additionally, faults show dip-slip motion, fault surfaces dip steeply and displace approximately horizontal layers. These combined factors provide an optimum situation for accurate measurement of fault parameters.

FAULT MEASUREMENT

Geometric and kinematic information on faults was obtained by mapping at a scale of 1:100 to 1:12,000. In many places, fault surfaces are well exposed so that fault parameters (e.g. strike and trace length) and direction of motion are actually measured rather than inferred from scarps (compare, for example, inferred dips and direction of motion of Dawers *et al.* 1993), computed from scan lines or maps (Walsh *et al.* 1991, Peacock & Sanderson 1994), or interpreted from seismic reflection profiles (Marrett & Allmendinger 1992). Displacements and lengths were measured directly from offset planar cooling unit boundaries within the Bandelier Tuff. Some information, gathered from exposures in fault-related saddles along mesas, provided three-dimensional control of fault surfaces. For each fault, displacement, strike, dip, thickness (normal to fault surface), length (along strike) and kinematic indicators were measured where possible. Trace lengths were determined for faults with lengths greater than 100 m. Trace lengths shorter than 100 m were typically difficult to determine accurately, and thus, are not included here. The magnitude of error associated with the lengths measured (i.e. lengths ≥ 100 m) is probably a few percent because fault terminations were commonly easily observed and

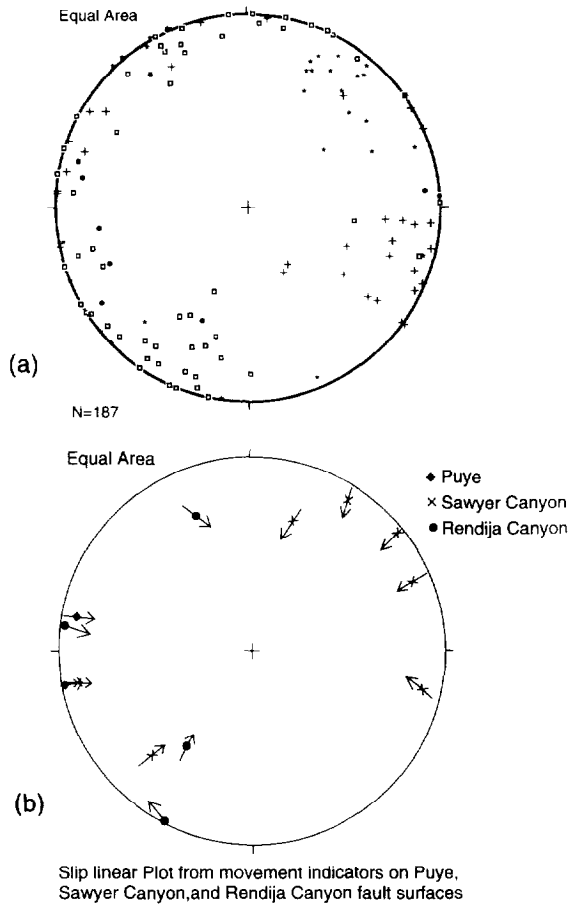

Fig. 3. Lower hemisphere equal area stereographic projections of faults in the western Española Basin. (a) Poles to fault surfaces: faults lettered a (box), b,c (dot), d (*), e (+). (b) Slip linear plot of kinematic indicators on fault planes: dot, + and ◆ represent pole to fault, arrow represents direction of movement on fault.

mapped at a detailed scale. Displacements on 'small' ($\leq$3 m) faults were measured directly with a tape measure and probably have no significant errors. Larger displacements ($\geq$3 m) were measured by standard leveling techniques using a Brunton compass. Any error associated with these displacements would be related to the precision of the Brunton compass: careful leveling probably resulted in errors of 0 to 0.1 m for these displacements.

Ninety individual faults associated with five major fault zones were measured by two-dimensional sampling. Because most of the faults have short lengths and small displacements (see next section), only one displacement was measured on each fault. For the five largest faults, however, displacements were measured in several places along each trace to assess their displacement profiles. Only the maximum displacement obtained for each of these faults is used in the distribution analysis (see below) so that the sampling dimensions are comparable for faults with displacements of all magnitudes (see Marrett & Allmendinger 1991). All faults dissect the Bandelier Tuff and most displace sedimentary deposits overlying the Tuff. Faults trend roughly north and dip steeply east or west (Fig. 3a). Slickensided surfaces reveal exclusively normal motion on all but part of one minor slip surface near a fault tip (Fig. 3b).

Recent reports suggest that to assess accurately the dimensional relationships of faults, fault dimensions should span several orders of magnitude and comprise a single data set (see, for example, Childs *et al.* 1990, Cowie & Scholz 1992b, Gillespie *et al.* 1992). Further, Wojtal (1994) even suggests separating single data sets from mature fault systems into groups based on different fault magnitudes to examine more accurately the dynamics of the population. Faults in this study have displacements that span five-orders of magnitude and comprise an immature fault system that occurs in a single, small tectonic environment. Therefore, this should be one of the best data sets with which to determine the nature of the population: for example, the characteristic fractal dimension and scaling relationship. Additionally, in the past 1.2 Ma, this region has experienced only one phase of tectonic deformation which should simplify interpretation of fault patterns and resultant strains (see, for example, Peacock & Sanderson 1994). Ultimately, characterizing these faults should help further understanding of continental rift faults and advance ideas on fault growth models.

FAULT POPULATION AND DIMENSIONS

To characterize this suite of faults fully, we present the size frequency distribution of fault displacements, the displacement-length correlation and the displacement profiles along individual faults.

Displacement population

A population of faults can be visualized with a fault displacement population plot which compares maximum displacement on a fault trace, d_{max}, with the number of faults with maximum displacement greater than, or equal to d_{max}, as shown in Fig. 4. The large range of displacements and large number of faults yields a reasonably complete curve that shows a straight-line segment (a of Fig. 4) for faults with small d, and a segment of steeper slope at higher values of d (b of Fig. 4). The straight-line segment (a) is a reflection of an unavoidable sampling bias ('truncation' of Jackson & Sanderson 1992). This bias necessarily occurs because 100% of the faults that exist in an area cannot be observed unless there is 100% three-dimensional exposure. This is clearly supported by the large number of faults with small ($\leq$1 m) displacements exposed in road cuts that would otherwise have escaped observation. Additionally, faults with very small displacements will likely escape observation if d is much smaller than bed thickness. Faults in this category are termed 'small' because they are not observable at a mappable scale for the given region and will, therefore, be underrepresented. On this basis, it is assumed that the population of faults with displacements less than a few meters is much larger than that measured, and that the straight-line segment (a) is unrepresentative of the fractal nature of faults in the western Española Basin. This problem is

not unique to this study, as it is similar to the hyperbolic tails observed by Lovejoy & Mandelbrot (1985) and by Mandelbrot (1967), who could not obtain an exact value for the length of a coast line because of millimetric-scale irregularities (see Turcotte 1992). At the moment, work is in progress (Carter in preparation) to explore fractional sampling that could further the understanding of this sampling bias.

The steep part (b) of the slope in Fig. 4, on the other hand, represents faults with displacements greater than approximately 1 m. Because faults of this size are easily detectable at the detailed level of mapping done in this study, it is unlikely that a significant number of faults of that magnitude were not measured. The completeness in representation of faults in this size range suggests that their population can be used to determine D, the fractal dimension of the fault set. The fractal dimension, in this case, is a means to quantify how faults at one scale relate to faults at a different scale: it is essentially the slope of the logarithm of the power-law curve for the size-frequency distribution (see next section). Although it remains unclear if D characterizes the entire fault population, it is certain that the number of small faults is larger than that which can be documented and, therefore, the slope of the straight-line segment (a) should be steeper, similar to D of the steeper segment (lines u, v or x, of Fig. 4).

Statistical evaluation of displacement data. Figure 5 shows displacements for 32 of the largest faults. The distribution of these data appears to be heavy-tailed in the sense that a disproportionate amount of total displacement is contributed by a few very large faults. For instance, the largest fault has a displacement that is about the same size as the sum of the other displacements. Furthermore, the largest displacement is more than five sample standard deviations from the sample mean, an event that would occur about three times in 10,000,000 if the data were normally distributed.

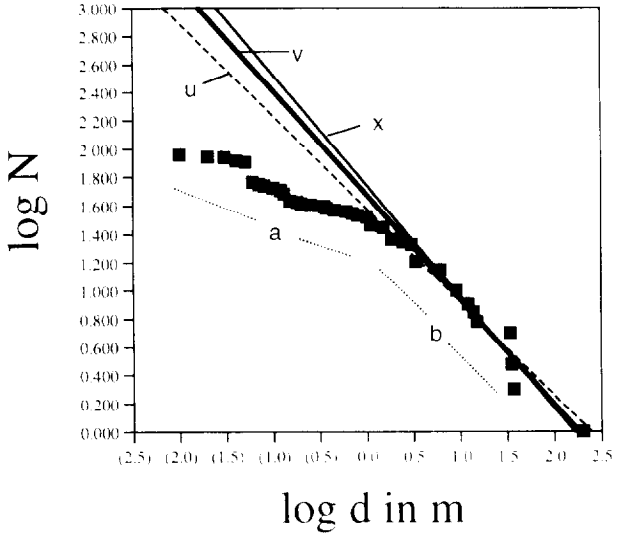

Fig. 4. Fault displacement population plot. N = number of faults with displacement $\geq d$. Population obeys a power-law size distribution. The slopes, which represent the fractal dimension, D, [see text equation (2)] are 0.66 (line u); 0.74 (line v); and 0.79 (line x). Log N_{actual} = 1.96, which is the number of actual faults measured with $d \geq 0.01$ m. Log $N_{extrapolated}$ = 3.5 which is the number of faults with $d \geq 0.01$ m, predicted to exist based on the extrapolation of the slope to its intercept at the abssisa. Negative numbers shown in parentheses.

We model $N(r)$, the number of faults with displacement greater than r, by a hyperbolic distribution,

$$N(r) = \alpha r^{-D}, \tag{1}$$

because it is heavy-tailed. α and D are constants that we estimate below. α indicates the number of displacements greater than one.

D is called the fractal dimension of $N(r)$(Mandelbrot & Wallace 1968) and the hyperbolic distribution is statistically self-similar in the sense of Mandelbrot (1982); that is, $N(\lambda r) = \lambda^{-B} N(r)$ (for an arbitrary constant, λ). When $D < 1$, hyperbolic distributions are so long-tailed that their ensemble mean and variance are infinite, which indicates that there are effectively no limits on the expected size of displacement or on their variance.

We estimate D and α by least squares regression of $\log N(r)$ against $\log r$,

$$\log N(r) = \log \alpha - D \log r. \tag{2}$$

In fact, we performed three different regressions because of uncertainty of the smallest displacement representing the lower limit of the 'large' fault set, and there is apparently no strong theory to establish the cutoff. For the first regression (u of Fig. 4) we used the group of 32 faults with displacements greater than 1 m which is the displacement corresponding to the change in slope. The second and third regressions (v and x of Fig. 4) consisted of 20 displacements greater than 3 m, and 13 displacements greater than 6 m, respectively. The limits of these two groups were chosen based on the confidence with which we believed we could certainly recognize the minimum displacement at the scale of mapping. It is unlikely that faults with $d \leq 3$ m were not measured, and even more unlikely that any faults with $d \leq 6$ m escaped measurement. The regressions on those groups, therefore, are valid representations of the majority of this fault population. Results are shown in Table 1.

The fit of all three equations is very good: correlations are high and the F-tests for $D = 0$ are highly significant indicating a strong linear relation between logarithm of displacement and logarithm of numbers of faults. Values of $\log \alpha$ are reasonably close across all three regressions; note that they yield expected values of $N(1) = \alpha$ between about 37 and 55, which are reasonably near 32, the number actually observed.

Values of D do not appear significantly different. We calculated confidence intervals for them (Table 2) for two reasons: first, D controls the statistical properties of $N(r)$. We are especially interested to see whether D is significantly less than 1, in which case, the tails of $N(r)$ are quite heavy. Table 2 indicates that this is so for all three samples. Second, we want to see whether the confidence intervals overlap. Because Table 2 indicates that they do, we conclude that the selection of the sample does not critically affect our estimates of D. It is,

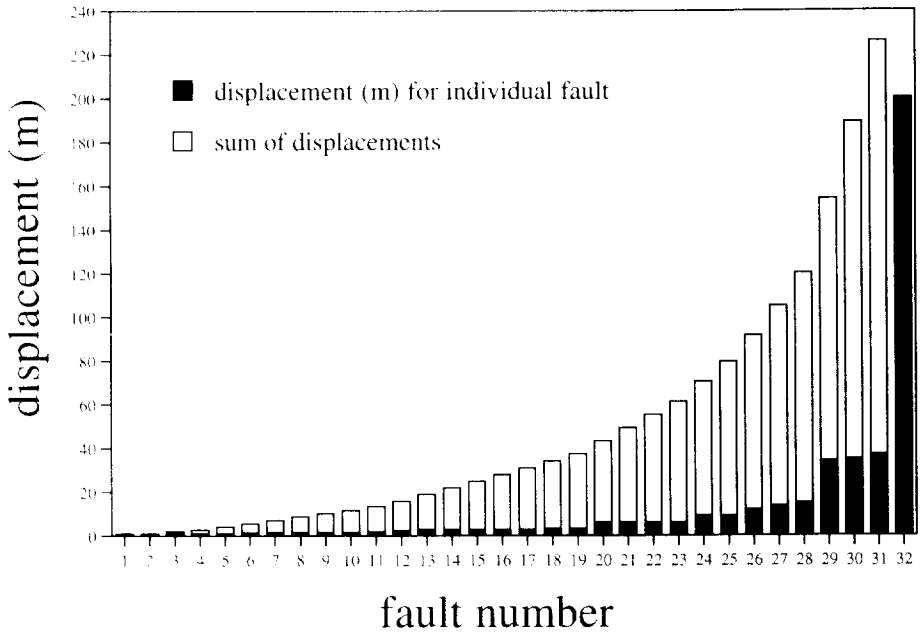

Fig. 5. Cumulative fault displacement data for faults with $d_{max} \geq 1$ m. Solid bars indicate displacement for a single fault, d_n; open bars indicate cumulative fault displacement for faults with $d_{max} \leq d_n$.

Table 1. Regression statistics

Smallest displacement in sample (m)	Log α	D	Correlation coefficient	F	Degrees of freedom
1	1.58	0.66	0.96	762	30
3	1.67	0.74	0.96	445	18
6	1.74	0.79	0.95	208	11

therefore, reasonable to suggest that the value of D is somewhere around 0.74 and this is geologically supported in that the minimum cutoff displacement values (3 m, 6 m) for the two data sets yielding $D = 0.74$ and $D = 0.79$, would be reasonably easy to detect in the field, compared to that (1 m) from which $D = 0.66$ was derived.

It is interesting to see how heavy the tails of $N(r)$ are with the values of log α and D in Table 1. For displacements of 200 m, the size of the largest displacement $N(200) = 1.15$ for log $\alpha = 1.58$ and $D = 0.66$. $N(200) = 0.91$ for log $\alpha = 1.67$ and $D = 0.74$. $N(200) = 84$ for log $\alpha = 1.74$ and $D = 0.79$. These are in very good agreement with the actual number, 1, of displacements $\geq$200 m. (Note: log $N_{actual} = 1.96$, which is the number of actual faults measured with $d \geq 0.01$ m. Log $N_{extrapolated} = 3.5$ which is the number of faults with $d \geq 0.01$ m, predicted to exist based on the extrapolation of the slope to its intercept at the absissa on Fig. 4.)

Table 2. Confidence intervals for D

Estimate of D	Standard error of D	Lower bound of D	Upper bound of D
0.66	0.024	0.61	0.71
0.74	0.036	0.66	0.82
0.79	0.054	0.67	0.91

Displacement and length

The fault parameters discussed here include trace length, (L), maximum displacement on a fault trace, (d_{max}), and width (dimension parallel to the slip direction). The traces of all faults (except the Pajarito) are less than 8 km long, and most (84%) are shorter than 3 km (Fig. 6). The depths at which most faults terminate (i.e. maximum widths) are unknown. However, because fault a (Fig. 2) is steeply (ca. 70°) W-dipping (Fig. 3a), geometrically it could terminate at a depth of $\leq$2.5 km if it intersects the surface of the Pajarito fault. Based on this, and the short lengths of all faults, fault widths are assumed to be short.

Fault displacements and lengths are plotted in Fig. 6 and show a linear relationship which indicates that the ratio, d_{max}/L, is nearly constant. Cowie & Scholz (1992b) term this scaling parameter γ, and suggest that it depends on the shear strength, shear modulus and frictional resistance of the faulted host rock. For this data set, $\gamma = 5 \times 10^{-3}$ which, on a log–log plot (Fig. 6a), represents the best fit line of constant shear strain (Scholz & Cowie 1990). It is interesting that some of the largest faults have had several episodes of movement throughout the Quaternary (Gardner *et al.* 1990), yet γ is constant for these and smaller faults, some of which have probably moved only once (e.g. faults with $d \leq 1$ m).

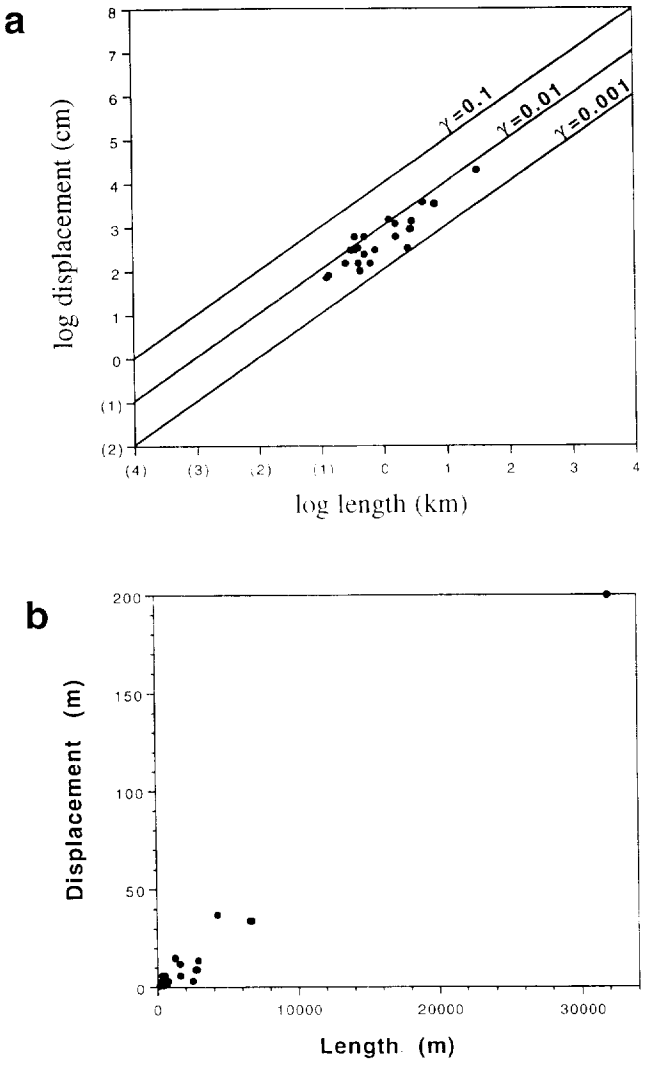

Fig. 6. (a) Log–log plots of maximum displacement and length. Log d_{max}/log L = 5 × 10^{-1} = scaling parameter γ. Solid lines are lines of constant γ. (b) Linear axis plots of displacement and length. Errors associated with displacement and length are not visible at the scale shown.

Displacement profiles

Displacement profiles for five faults (excluding the Pajarito) are shown in Fig. 7. These faults, which have curved traces at both ends, appear to be unsegmented continuous, individual surfaces. Lengths and displacements range from 3.25 to 10 km (Figs. 2, 6 and 7) and zero to 37 m (Figs. 4–7), respectively. The profiles show displacements only at points along a fault where vertical offset could be accurately measured. Displacement varies relatively systematically along the length of each fault: maxima occur away from the center of the fault and displacement decreases abruptly toward the fault tips. Near the tips of four of the longest faults, displacement is large (Fig. 7) and appears to be transferred into diffuse fractured zones. These zones have a higher fracture density compared to the surrounding host rock, and comprise sub-parallel fractures in a band parallel to, and wider than, the fault surface. The length of only three fault-tip fracture zones were measured (a, c & d of Fig. 2) because of the difficulty in judging accurately the decreasing density of fractures as the zone diffuses into the host rock away from the fault tip. Fracture zone lengths are estimated to be 0.36, 0.4 and 0.29 for faults a, c and d (Fig. 2), respectively.

INTERPRETATION AND IMPLICATIONS FOR STRAIN

Analysis of faults in the Española Basin, using fault populations, dimensional relationships and displacement profiles shows that the faults have a fractal size distribution, a linear relationship between displacement and length, and varying displacement gradients along the fault traces.

Fault displacement population

Faults in this population appear the same at different scales and displacements obey a power-law, or hyperbolic, distribution (see Fig. 4 and previous section). Therefore, these faults are scale-invariant, for the range mapped, and are considered to be fractal in nature. Scaling of the self-similar behavior is quantified by the fractal dimension, D, which, for these faults, is between 0.66 and 0.79 [equation (2) and Fig. 4]. This behavior exists over at least two, and probably over five-orders of magnitude, which is further indication that faulting, here, is scale-invariant. Similar conclusions for other data sets have been controversial, in part because of limited range of scale, small fault population, and data collection biases (see Cowie & Scholz 1992b). Turcotte (1989, p. 173), for example, proposes that 'under some circumstances, different fractal scaling may be applicable at different scales'. Barton & Zoback (1992) suggest that there may be only a limited range over which self-similar behavior can be assured. In part, questions regarding the different scaling relationships

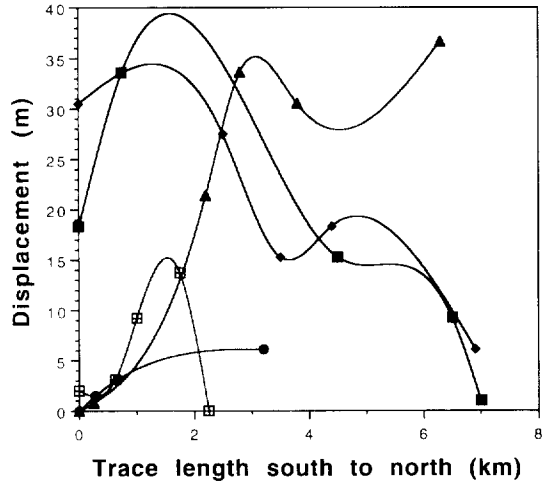

Fig. 7. Fault displacement (d_{max}) profiles (smoothed) for faults a through c of Fig. 2. Note asymmetric distribution and abrupt decrease in displacement at fault terminations. Errors associated with displacement measurements are not visible plotted at this scale.

between large and small faults could reflect tectonic environment and incompatible data from combined data sets as pointed out by Cowie & Scholz (1992b) and Wojtal (1994). For this intimately known, carefully gathered data set, small faults are known to be underrepresented (see previous section) and cannot be assumed to obey the same fractal scaling as large faults. However, because the population of small faults must be larger than measured, slope a of Fig. 4 must be steeper, although we cannot, at present, determine an accurate fractal dimension for just this part of the population. We can, however, reasonably and conservatively suggest that the fractal dimension of such small faults must be closer to that for larger faults ($D \leq 0.74$, see Fig. 4). Implications, therefore, are that, within this active, immature tectonic region, faulting appears to be scale invariant (at least for faults with $d > 1$ m and probably for the entire population), and that the distribution can be described by a single fractal dimension.

The scale-invariant relationship of faults has implications for estimating total strain in this region. Several authors (e.g. Scholz & Cowie 1990, Walsh *et al.* 1991, Marrett & Allmendinger 1991, 1992), suggest that if fault data show a power-law relationship, total strain can be estimated. Further, if d and l are systematically related, Marrett & Allmendinger (1991) provide a method to estimate two-dimensional strain through summation of the geometric moment of faults. Using equations (6b) and (14) (Marrett & Allmendinger 1991, p. 736), in which $c_1 = 0.74$ and $c_2 = 1$ for this population, the total geometric movement is 221.66 km^3. Total strain across this area, then, using equation (11) from Westaway (1994) is 5.04%. If the contribution of unobserved faults were not considered, and strain were calculated based solely on the observed displacements, the two-dimensional strain across the region would have been 4.75%. For this region, then, it appears that the contribution of small unobserved faults to the total strain is small, accounting for at most 6% of the total strain.

That the contribution of unobserved faults, determined by extrapolation, is small does not resolve the conflict of whether small faults can be neglected in a regional strain estimate (see Scholz & Cowie 1990, King & Cisternas 1991, Walsh *et al.* 1991, Marrett & Allmendinger 1992). Rather, in this case, the apparently small contribution to strain from faults near the limit of resolution ($d \leq 1$ m) probably reflects two things: (1) Faults in this size fraction are becoming less important as the fault system evolves; faults with $d \geq 1$ m could be accommodating progressively more strain as larger faults play a more dominant role. (2) Because many faults with displacements as small as $d \leq 0.01$ m were actually measured in this area, they do not constitute part of the 'unobserved' fraction. Therefore, the unobserved fraction is smaller than that which would have resulted if none of those small faults had been fortuitously exposed in road cuts and construction sites. This conclusion does not suggest that small faults are unimportant in other regions where mapping might be at a different scale (e.g. faults with $d \leq 1$ m are not mapped), or faults are reactivated, or exist in a different tectonic setting. Further, it can be speculated that the contribution of 'small' faults to this population might be similar to that in other relatively simple active continental rift zones where faults are young and unreactivated.

Displacement and length relationship

Faults in this region show a linear relationship between displacement and length, which is consistent with theoretical results which show that, for single data sets, d_{max} and L are linearly related. The scaling parameter, γ, (slope with line in Fig. 6a) for this relationship is 5×10^{-3}. In the model of Cowie & Scholz (1992a,b), the constant of proportionality depends on the remote shear stresses and host rock properties shear strength, shear modulus and frictional resistance. According to their inelastic model of deformation, Cowie & Scholz (1992a,b) suggest that d_{max}/L will be large for host rocks with large shear strengths, small shear moduli and small frictional resistance. Assuming their models are correct (i.e. that d_{max}/L is dependent on host rock properties and tectonic environment), faults in the western Española Basin should provide information about the host rock as well as a standard for scaling of normal faults in an active continental rift.

All faults, except the major western margin (Pajarito) fault have small ratios of d_{max}/L and lengths of 8 km or less, and more than 84% of these faults have traces shorter than 3 km. Based on models of Cowie & Scholz (1992b), these dimensions, combined with the inferred width of fault c of Fig. 2a (see previous section on displacement and length), suggest that faults probably do not span the brittle crust and that host rocks in this region have a collectively low shear strength, large shear modulus and high frictional resistance. If remote shear stresses were relatively constant throughout faulting, these host rock properties should characterize those of the mixed volcanic, volcaniclastic and sedimentary packages in this area (Fig. 2).

It is interesting that the scaling relationship for faults in this region appears to be valid over a wide range (length = 100 m to 35 km) of fault sizes. This has also been noted by a few others (e.g. Dawers *et al.* 1993); however, many authors recently have suggested that large and small faults might obey different scaling laws. Scholz & Aviles (1986) note that large earthquakes are not self-similar with small earthquakes and suggest the term 'fractal tear' to describe the hierarchical jump between them (thereby inferring a similar relationship between the seismogenic faults). Turcotte (1989) speculates that different fractal scaling might be applicable at different scales under some circumstances. Cowie & Scholz (1992b) suggest that faults not spanning the brittle crust might scale differently from faults that do span the crust. The nearly constant ratio ($\log d_{max}/\log L$) for Española Basin faults, therefore, is probably indicative of a particular fault growth history in which there is a relationship between successive stages of

growth of individual faults. Because $\log d_{max}/\log L$ is the same for faults known to have experienced different numbers and amounts of movement, that ratio necessarily reflects a different stage of development for each individual fault. This strongly suggests that, for these faults, displacement and length have increased proportionately during each growth increment. In terms of length, this is consistent with the idea of Cowie & Scholz (1992c) that 'increase in the length of a fault in an earthquake that ruptures the entire fault is a constant proportion, r, of its previous length'. By virtue of the scaling relationship of d_{max}/L in this data set, the same basic relationship must be true of displacement. That is, each increment of d must be a constant proportion of its previous magnitude.

Although $\log d_{max}/\log L$ is nearly constant for this data set, suggesting that similar faulting mechanisms were active during the evolution of each individual fault, there is some scatter that might reflect sampling artifacts or particular growth mechanisms. This scatter should be expected considering the number of variables that could affect this ratio (d_{max}/L). For example, the scatter could reflect the different dimensions of chords (see Walsh & Watterson 1988) across different parts of fault surfaces, different earthquake focal depths, non-uniform slip distributions along a fault surface, and different slip distributions along different faults. Alternatively, if faulting was dominated by linking of relatively short fault segments, faults might disproportionately increase in length compared to displacement (assuming systematic linkage), thereby creating a distribution of faults with a trend away from the line 5×10^{-3} in Fig. 6(a). There is, however, no systematic variation within the scatter rendering it unlikely that a particular process, such as systematic fault-linkage, created the observed scatter. Lastly, it might simply be that the minor scatter of some points in Figs. 6(a) & (b) reflects fault tip growth into a different (subsurface) host rock, that faults nucleated at different depths or remote shear stress and shear resistance changed during the life of the faults. If any of these possibilities were significant factors, they would imply that individual faults experienced slightly different conditions at some point in their development compared to those faults with a better correlation coefficient to the line 5×10^{-3} in Fig. 6(a).

The relationship between $\log d_{max}$ and $\log L$ for Española Basin faults is similar to one other published data set: normal faults in coal beds in the British Coal Measures (Walsh & Watterson 1987) also show small ratios of d to L for faults of similar scale. If the scaling of displacement and length depends on rock properties and tectonic environment, then these similarities imply that the coal beds behaved much like the weak layered deposits in the Española Basin, or that the faults formed in a similar tectonic environment. Comparison of similarly scaled faults from different areas should be possible in more detail as data become available.

The dense fracture zones surrounding the terminations of at least five of the longest fault zones, might also hold information about the faulting process and host rock properties. This zone, termed the process zone, s, (Atkinson 1987, Scholz *et al.* 1993, also called 'break down zone' of Cowie & Scholz 1992a), comprises the zone of inelastic deformation localized near the fault termination where displacement decreases to near zero and the stress concentration at that point is accommodated by distributed fracturing rather than by sliding. For three of the longest faults, the process zone lengths range from 29% to 40% of the fault length, which is large compared to the general relationship of 10% to 20% reported for other data sets (Cowie & Scholz 1992a). Although only three zones were measured, it appears that s is relatively long and well developed for faults in this region, which implies that inelastic deformation dies out slowly at the fault tip and is spread throughout a large volume. According to models of Cowie & Scholz (1992a), such distributed deformation probably reflects generally weak host rocks (i.e. relatively low shear strengths and low frictional resistance) which is consistent with their idea that s is inversely proportional to shear strength (Cowie & Scholz 1992a).

Fault displacement profiles

Fault displacement profiles in Fig. 7 show an asymmetric distribution: the maximum displacement is not at the center of the fault trace and displacement drops off abruptly near fault terminations. Displacement at the tips of the two largest faults decreases abruptly from tens of meters to zero. The shape of the profiles neither supports nor precludes the suggestion (above) that these faults are self-similar. Faults could have initiated with, and maintained throughout their growth, a shape similar to their present geometry. In this case, successive rupture events would have increased displacements and lengths at roughly similar proportions after an initially asymmetric distribution was imprinted upon fault inception. Such a scenario is supported by the nearly constant ratio of d_{max}/L described in the previous section.

It is interesting that, for the faults profiled, there is a rapid decrease in displacement near the fault tip, indicative of strong host rocks, yet these faults also have small ratios of d_{max}/L, and, for three faults, relatively long process zones, which are indicative of weak host rocks (Cowie & Scholz 1992a). It is possible that, because the shape of s is unknown in three dimensions, its relatively long length might represent near surface distributed deformation that preferentially occurs in the weak upper layers of the host rock (Bandelier Tuff) on the two faults closest to the master fault.

CONCLUSIONS AND REGIONAL IMPLICATIONS

The fault population in the western Española basin shows a power-law, or fractal, size distribution which implies that faults are self similar and, therefore, scale invariant over at least three and probably five, orders of magnitude. The power-law nature can be statistically

addressed using fractal scaling relationships in which the fractal dimension, D, characterizes the linear segment of the power-law curve. For this population, fault groups were chosen by imposing statistical and geologic limits to calculate and statistically compare different fractal dimensions. Results yield values of D between 0.66 and 0.79, which is within the range of $0.37 \leq D \leq 1.7$ noted for other fault populations (see Marrett & Allmendinger 1992).

At present, it cannot be confirmed that this value is also characteristic of small unobserved faults in the area. Because a few road cuts fortuitously expose small faults that would otherwise have escaped measurement, it is suggested that the unobserved fault fraction would be characterized by a fractal dimension similar to, if not the same as, that of the observed population (see Fig. 4) (Carter in preparation). Accordingly, it is suggested that faults in this data set are scale invariant and that the fractal dimension necessarily represents a very young, probably immature, active fault population in a continental rift environment in which data were obtained by direct field measurement. It does not follow that this scaling relationship is representative of those characterizing mature strike slip or thrust fault systems (see Aviles *et al.* 1987 and Wojtal 1994, respectively) which could be governed by different energy and mechanical laws that, we believe, ultimately determine the fractal character of fragmentation processes, such as faulting. On the other hand, the relationship of this fractal dimension to other data sets in similar tectonic settings (i.e. active, immature extensional domains) is speculative: it could be suggested that a similar fractal dimension would be found if the same sampling procedures were employed.

Based on the fractal dimension of the population, the contribution to total extension from the unobserved fault fraction is approximately 6%. Considering the contribution from all faults, this area has extended at least 5% since 1.2 Ma.

Finally, a direct correlation between displacement and length of faults in this area suggests that they obey a scaling relationship in which the ratio, $\log d_{max}/\log L$, is 5×10^{-3}. This relationship is observed for faults over three orders of magnitude indicating that there is no difference in scaling between large and small faults in this region. If, as suggested by Cowie & Scholz (1992b), faults are loaded by a constant remote stress, d_{max} scales linearly with length and therefore, the scaling relationship of d_{max}/L relates to the host rock properties and tectonic environment. Moreover, this relationship helps constrain growth models. For this region, d_{max}/L is interpreted as reflecting: (1) low host rock shear strengths and/or high remote shear stresses; and (2) that most of the short (<7 km) faults do not extend throughout the brittle crust (see Cowie & Scholz 1992a,b). Because faults in this region have had several episodes of movement yet maintain a constant ratio of $\log d_{max}/\log L$, it is reasonable to suggest that displacement and length have increased proportionately during most growth increments. Moreover, the relative constancy (linear trend) of d_{max}/L and relative values of d_{max} to L could be consistent with faulting dominated by propagation of shear fractures rather than by systematic fault linkage.

The fractal nature of faults in the Española Basin is similar to that of faults in other regions and complements those data sets. The simple scaling relationship of these faults and its implications for fault growth processes could be representative of those for active faults in other extending regions.

Acknowledgements—We are grateful to P. Cowie, D. Turcotte and P. Gillespie for their insightful criticisms and thorough reviews which considerably improved the final draft. We are grateful to R. Marrett for his help with sampling dimensions and calculation of strain. We thank M. Krogh and J. Gardner for helpful discussions, and K. Wohletz for helpful comments on an early draft of the manuscript. KC acknowledges support from Los Alamos National Lab. and the Department of Energy administered through Oak Ridge Institute for Science and Education.

REFERENCES

Aldrich, M. J. 1986. Tectonics of the Jemez Lineament in the Jemez Mountains and Rio Grande rift. *J. geophys. Res.* **91**, 1753–1762.

Aldrich, M. J., Chapin, C. E. & Laughlin, A. W. 1986. Stress history and tectonic development of the Rio Grande rift, New Mexico. *J. geophys. Res.* **91**, 6199–6211.

Atkinson, B. K. 1987. *Fracture Mechanics of Rock*. Academic Press, Inc., London.

Aviles, C. A., Scholz, C. H. & Boatwright, J. 1987. Fractal analysis applied to characteristic segments of the San Andreas fault. *J. geophys. Res.* **92**, 331–344.

Bailey, R. A., Smith, R. L. & Ross, C. A. 1969. Stratigraphic nomenclature of volcanic rocks in the Jemez Mountains, New Mexico. *Bull. U.S. Geol. Surv.* **1274-P**.

Barton, C. A. & Zoback, M. D. 1992. Self similar distribution and properties of macroscopic fractures at depth in crystalline rock in the Cajon Pass scientific drillhole. *J. geophys. Res.* **97**, 5181–5200.

Carter, K. C. & Gardner, J. N. 1993. Quaternary fault kinematics in the Northern Española Basin, Rio Grande rift: implications for early rift development. *Eos. Trans. Am. Geophys. Union* **74**, 611.

Childs, C., Walsh, J. J. & Watterson, J. 1990. A method for estimation of the density of fault displacements below the limits of seismic resolution in reservoir formations. In: *North Sea Oil and Gas Reservoirs II* (edited by Buller, A. T. *et al.*). Graham & Trotman, London, 309–318.

Cowie, P. A. & Scholz, C. H. 1992a. Physical explanation for the displacement-length scaling relationship of faults using a post-yield fracture mechanics model. *J. Struct. Geol.* **14**, 1133–1148.

Cowie, P. A. & Scholz, C. H. 1992b. Displacement-length scaling relationship for faults: data synthesis and discussion. *J. Struct. Geol.* **14**, 1149–1156.

Cowie, P. A. & Scholz, C. H. 1992c. Growth of faults by seismic slip. *J. geophys. Res.* **97**, 11,085–11,096.

Dawers, N. H., Anders, M. H. & Scholz, C. H. 1993. Growth of normal faults: Displacement-length scaling. *Geology* **21**, 1107–1110.

Gardner, J. N. & Goff, F. 1984. Potassium–argon dates from the Jemez volcanic field: Implications for tectonic activity in the north-central Rio Grande rift. *New Mexico Geol. Soc. Guidebook* **35**, 75–81.

Gardner, J. N., Goff, F., Garcia, S. & Hagan, R. 1986. Stratigraphic relations and lithologic variations in the Jemez Volcanic Field, New Mexico. *J. geophys. Res.* **91**, 1763–1778.

Gardner, J. N. & House, L. 1987. Seismic Hazards Investigations at Los Alamos National Laboratory, 1984–1985. Los Alamos Sci. Lab. Rep. LA11072-MS.

Gardner, J. N., Baldridge, W. S., Gribble, R., Manley, K., Tanaka, K., Geissman, J. W., Gonzalez, M. & Baron, G. 1990. Results from seismic hazards trench 1 (SHT-1) Los Alamos Seismic Hazards Investigations. Los Alamos Nat. Lab. Rep. EES1-SH90-19.

Gillespie, P. A., Walsh, J. J. & Watterson, J. 1992. Limitations of dimension and displacement data from single faults and the consequences for data analysis and interpretation. *J. Struct. Geol.* **14**, 1157–1172.

Hatton, C. G., Main, I. G. & Meredith, P. G. 1993. A comparison of seismic and structural measurements of scaling exponents during tensile subcritical crack growth. *J. Struct. Geol.* **15**, 1485–1495.

Izett, G. A. & Obradovich, J. D. 1994. $^{40}Ar/^{39}Ar$ age constraints for the Jaramillo Normal Subchron and the Matuyama–Brunhes geomagnetic boundary. *J. geophys. Res.* **99**, 2925–2934.

Jackson, P. & Sanderson, D. J. 1992. Scaling of fault displacements from the Badajoz–Cordoba shear zone, SW Spain. *Tectonophysics* **210**, 179–190.

King, G. & Cisternas, A. 1991. Geological faulting: Do little things matter? *Nature* **351**, 350.

Lovejoy, S. & Mandelbrot, B. B. 1985. Fractal properties of rain, and a fractal model. *Tellus* **37A**, 209–232.

Mandlebrot, B. B. 1967. How long is the coast of Britain? Statistical self-similarity and fractional dimension. *Science* **156**, 636–638.

Mandlebrot, B. B. 1982. *The Fractal Geometry of Nature*. W. H. Freeman, San Fransisco.

Mandelbrot, B. B. & Wallis, J. R. 1968. Noah, Joseph and operational hydrology. *Wat. Resour. Res.* **4**, 909–918.

Manley, K. 1979. Stratigraphy and structure of the Española Basin, Rio Grande rift, New Mexico. In: *Rio Grande Rift: Tectonics and Magmatism* (edited by Riecker, R. E.). *Am. Geophys. Union*, Washington, D.C., 71–86.

Marrett, R. A. & Allemdinger, R.W. 1991. Estimates of strain due to brittle faulting: sampling of fault populations. *J. Struct. Geol.* **13**, 735–738.

Marrett, R. A. & Allmendinger, R. W. 1992. Amount of extension on 'small' faults: An example from the Viking Graben. *Geology* **20**, 47–50.

Peacock, D. C. P. & Sanderson, D. J. 1994. Strain and scaling of faults in the chalk at Flamborough Head, U.K. *J. Struct. Geol.* **16**, 97–107.

Scholz, C. H. & Aviles, C. A. 1986. The fractal geometry of faults and faulting. In: *Earthquakes Source Mechanics* (edited by Das, S. *et al.*) *Am. Geophys. Union Monogr.* **37**, 147–156.

Scholz, C. H. & Cowie, P. 1990. Determination of total strain from faulting. *Nature* **346**, 837–839.

Scholz, C. H., Dawers, N. H., Yu, J.-Z., Anders, M. H. & Cowie, P. A. 1993. Fault growth and fault scaling laws: Preliminary results. *J. geophys. Res.* **98**, 12951–12961.

Turcotte, D. L. 1986. A fractal model for crustal deformation. *Tectonophysics* **132**, 261–269.

Turcotte, D. L. 1989. Fractals in geology and geophysics. *Pure & Appl. Geophys.* **131**, 171–196.

Turcotte, D. L. 1992. *Fractals and Chaos in Geology and Geophysics*. Cambridge University Press, Cambridge.

Walsh, J. J. & Watterson, J. 1987. Distributions of cumulative displacement and seismic slip on a single normal fault surface. *J. Struct. Geol.* **9**, 1039–1046.

Walsh, J. J., Watterson, J. & Yielding, G. 1991. The importance of small-scale faulting in regional extension. *Nature* **351**, 391–393.

Watterson, J. 1986. Fault dimensions, displacements and growth. *Pure & Appl. Geophys.* **124**, 365–373.

Wojtal, S. F. 1994. Fault scaling laws and the temporal evolution of fault systems. *J. Struct. Geol.* **16**, 603–612.